Effects of number of parallel runs and frequency of bias-strength replacement in generalized ensemble molecular dynamics simulations

Takuya Shimato [Equal first author, 1] , **Kota Kasahara** [Corresp., Equal first author, 2] , **Junichi Higo** [3] , **Takuya Takahashi** [2]

1 Graduate School of Life Sciences, Ritsumeikan University, Kusatsu, Shiga, Japan

2 College of Life Sciences, Ritsumeikan University, Kusatsu, Shiga, Japan

3 Graduate School of Simulation Studies, University of Hyogo, Kobe, Hyogo, Japan

Corresponding Author: Kota Kasahara
Email address: ktkshr@fc.ritsumei.ac.jp

Background. The generalized ensemble approach with the molecular dynamics (MD) method has been widely utilized. This approach usually has two features. (i) A bias potential, whose strength is replaced during a simulation, is applied. (ii) Sampling can be performed by many parallel runs of simulations. Although the frequency of the bias-strength replacement and the number of parallel runs can be adjusted, the effects of these settings on the resultant ensemble remain unclear.

Method. In this study, we performed multicanonical MD simulations for a foldable mini-protein (Trp-cage) and two unstructured peptides (8- and 20-residue poly-glutamic acids) with various settings.

Results. As a result, running many short simulations yielded robust results for the Trp-cage model. Regarding the frequency of the bias-potential replacement, although using a high frequency enhanced the traversals in the potential energy space, it did not promote conformational changes in all the systems.

1 Effects of number of Parallel Runs and Frequency of
2 Bias-Strength Replacement in Generalized Ensemble
3 Molecular Dynamics Simulations.

6 **Takuya Shimato,**[1,†] **Kota Kasahara,**[2,†,*] **Junichi Higo**[3]**, and Takuya Takahashi**[2]

8 *Graduate School of Life Sciences, Ritsumeikan University, Kusatsu, Shiga, Japan*
9 *College of Life Sciences, Ritsumeikan University, Kusatsu, Shiga, Japan*
10 *Graduate School of Simulation Studies, University of Hyogo, Kobe, Hyogo, Japan*
11 † The first two authors are considered to be joint first authors.

13 Corresponding Author:
14 Kota Kasahara
15 *Graduate School of Life Sciences, Ritsumeikan University, 1-1-1 Noji-higashi, Kusatsu, Shiga,*
16 *Japan 525-8577*
17 Email address: ktkshr@fc.ritsumei.ac.jp

20 Abstract

21 **Background.** The generalized ensemble approach with the molecular dynamics (MD) method
22 has been widely utilized. This approach usually has two features. (i) A bias potential, whose
23 strength is replaced during a simulation, is applied. (ii) Sampling can be performed by many
24 parallel runs of simulations. Although the frequency of the bias-strength replacement and the
25 number of parallel runs can be adjusted, the effects of these settings on the resultant ensemble
26 remain unclear.
27 **Method.** In this study, we performed multicanonical MD simulations for a foldable mini-protein
28 (Trp-cage) and two unstructured peptides (8- and 20-residue poly-glutamic acids) with various
29 settings.
30 **Results.** As a result, running many short simulations yielded robust results for the Trp-cage
31 model. Regarding the frequency of the bias-potential replacement, although using a high
32 frequency enhanced the traversals in the potential energy space, it did not promote
33 conformational changes in all the systems.

34

35 Introduction

36 In the past several decades, the molecular dynamics (MD) method has been widely applied to
37 investigate the microscopic behavior of molecular systems. Although advances in high-
38 performance computing technology have extended the timescale that is reachable by MD

39   simulations (Salomon-Ferrer et al., 2013; Shaw et al., 2014; Abraham et al., 2015), there is still a
40   large gap from experimental measurements. In particular, it is not straightforward to characterize
41   the free-energy landscape (FEL) of a complex molecular system, because the characteristics of
42   conformational ensembles obtained via canonical MD simulations largely depend on the initial
43   conditions. To solve this problem, the generalized ensemble (GE) approach has been extensively
44   developed and applied to the MD method. The GE approach enhances the conformational
45   sampling using some tricks. First, in many GE methods, the conformational sampling can be
46   performed with many parallel runs of simulations in a coupled or independent manner. For
47   example, the replica-exchange MD (REMD) method (Sugita & Okamoto, 1999) involves
48   performing many simulations of the same system, i.e., replicas, with different temperatures. The
49   replicas with adjacent temperatures are coupled by exchanging their temperatures via Monte
50   Carlo trials. On the other hand, the multicanonical MD (McMD) method (Nakajima, Nakamura
51   & Kidera, 1997) can be performed by multiple independent runs, and a resultant ensemble is
52   obtained by concatenating the trajectories of these runs (Ikebe et al., 2010). Second, the GE
53   approach generates a non-Boltzmann distribution by applying bias potential, e.g., heating/cooling
54   in the entire system or a part of the system, scaling the potential energies, and applying spring
55   potentials for parts of system. These biases enhance the conformational changes of molecules
56   and avoid trapping the molecular system at local minima in the FEL. During a simulation, the
57   strength of the bias is frequently replaced, and the system alternates between different bias
58   conditions. After simulations, a canonical ensemble can be obtained by reweighting each
59   snapshot in the sampled conformational ensemble (Souaille & Roux, 2001; Shirts & Chodera,
60   2008).
61   For using these two features, users must adjust some settings. First, the number of runs is
62   an adjustable parameter. In the case of the REMD method, using a larger number of replicas
63   allows wider overlaps of the energy distributions between adjacent replicas and results in a
64   higher acceptance probability. However, increasing the number of runs proportionally increases
65   the computational costs. Users must choose the optimal balance between the number of runs and
66   the length of each run according to the available computational resources. Previously, Ikebe et al.
67   reported that an increase in the number of independent runs of McMD yields efficient
68   exploration of a wider area of the conformational space. (Ikebe et al., 2010) However, the
69   balance between the number of runs and the length of each run has not been discussed. Second,
70   the frequency of the bias-strength replacement is also adjustable. In the REMD method, the
71   frequency of replica-exchange trials must be specified by users. Other methods using a
72   continuous bias strength, e.g., McMD and adaptive umbrella sampling (AUS), can control the
73   frequency of bias-strength replacement by using the virtual-system coupling scheme, (Higo,
74   Umezawa & Nakamura, 2013; Higo et al., 2015) as described later. It is reported that the
75   frequency of the bias-strength replacement affects the resultant ensembles for the REMD
76   method. (Periole & Mark, 2007; Sindhikara, Meng & Roitberg, 2008; Rosta & Hummer, 2009;
77   Sindhikara, Emerson & Roitberg, 2010; Jani, Sonavane & Joshi, 2014; Iwai, Kasahara &
78   Takahashi, 2018) Although higher frequencies enhance the traversals in the temperature space,

79 they are suspected as an origin of artifacts. Although the effects of these features have been
80 examined, these studies were mainly based on simple model peptides with helix–coil transitions.
81 The effects of the features for more practical cases, e.g., a protein folding–unfolding transition,
82 are not fully understood. More importantly, the relationship between these effects and the
83 complexities of molecular systems, e.g., the degree of freedom and ruggedness of the free-energy
84 landscape, are expected to be revealed.
85 In this study, we aim to elucidate the effects of the number of runs and the bias-replacing
86 frequency for the GE method on the resultant conformational ensembles of molecular models
87 including a foldable mini-protein and disordered model peptides. We utilized the trivial-
88 trajectory parallelized virtual-system coupled McMD (TTP-V-McMD) method (Ikebe et al.,
89 2010; Higo, Umezawa & Nakamura, 2013), which is a variant of the McMD method, for
90 simulating the three molecular models with an explicit solvent: (i) Trp-cage, (ii) 8-residue poly-
91 glutamic acid (PGA8), and (iii) 20-residue poly-glutamic acid (PGA20). We chose these models
92 as test cases to examine the simulation conditions because they are sufficiently small for
93 elucidating their conformational ensembles within a practical computational time in addition to
94 the fact that their structural properties have been well studied thus far. Trp-cage, which is a mini-
95 protein consisting of 20 amino acids, has been widely studied as a prominent model of protein
96 folding. (Ahmed et al., 2005; Péter Hudáky et al., 2007; Hałabis et al., 2012) Poly-glutamic acids
97 have been used as model peptides to characterize the conformational properties of polypeptides.
98 (Clarke et al., 1999; Kimura et al., 2002; Finke et al., 2007; Donten & Hamm, 2013; Ogasawara
99 et al., 2018) We analyzed their FELs under various parameter settings to provide a guide for
100 adjusting these parameters for the GE methods. The questions to be answered are as follows:
101 "Which condition is more efficient: many short simulations or a small number of long-term
102 simulations?" and "Which is better: frequent or less frequent replacement of the bias strength?".
103 Moreover, we discuss the relationship between the relaxation of the energy and that of the
104 protein conformation. While the McMD method enhances the relaxation in the energy space, it is
105 not guaranteed to enhance the relaxation in the conformational space. We analyzed these two
106 relaxation processes using the McMD trajectories calculated with the various settings.
107

Materials & Methods

109 We calculated the FELs of the three explicitly solvated molecular models: Trp-cage, PGA8, and
110 PGA20, by using the TTP-V-McMD method with various settings. The theory of McMD,
111 virtual-system coupled McMD (V-McMD), and trivial-trajectory parallelization (TTP) is briefly
112 presented in the following subsections. Then, the simulation protocol applied in this study is
113 described.
114

McMD

116 The McMD method efficiently explores the conformational space of a molecular system, by
117 applying a biasing energy term. The Hamiltonian H of the system is
118 $$H = K + E_{mc}, \qquad\qquad (1)$$

119 where K and E_{mc} denote the kinetic energy and multicanonical energy, respectively. E_{mc} is
120 defined as follows:

121 $$E_{mc} = E + RT\ln P_c(E,T), \qquad (2)$$

122 where E is the potential energy, and the second term corresponds to the bias potential. R is the
123 gas constant, and $P_c(E, T)$ denotes the canonical distribution at the temperature T:

124 $$P_c(E,T) = \frac{n(E)\exp\left(-\frac{E}{RT}\right)}{Z_c(T)}, \qquad (3)$$

125 where $n(E)$ denotes the density of states, and $Z_c(T)$ is the partition function of the canonical
126 distribution at the temperature T. With this definition, the potential energy distribution of an
127 ensemble obtained from the McMD, or the multicanonical distribution, $P_{mc}(E)$, becomes
128 uniform:

129 $$P_{mc}(E) = \frac{n(E)\exp\left(-\frac{E_{mc}}{RT}\right)}{Z_{mc}(T)} = \frac{n(E)\exp\left(-\frac{E}{RT}\right)}{P_c(E,T)\,Z_{mc}(T)} = \frac{Z_c(T)}{Z_{mc}(T)} = const.$$

130 $\qquad (4)$

131 As a result, the McMD method performs a random walk in the potential energy space and
132 generates a uniform distribution of potential energy in a resultant ensemble. After a
133 multicanonical ensemble is obtained, a canonical ensemble at any temperature in a sampled
134 energy range can be generated by reweighting the probability of existence of each snapshot.
135 Eqs. (3) and (4) include an analytical form of $n(E)$, which is usually unknown *a priori*.
136 Therefore, $n(E)$ is approximated as a parametric function, e.g., the polynomial function, and its
137 parameters are estimated by iterations of McMD simulations to make $P_{mc}(E)$ near-uniform. In the
138 i^{th} iteration, the bias potential is calculated using Eq. (2) with the canonical distribution obtained
139 from the $(i–1)^{th}$ iteration, i.e., $P_c^{i-1}(E,T)$. As the result of the ith iteration, we obtain $P_{mc}^i(E)$. P_c^i
140 (E,T) can be calculated as

141 $$P_c^i(E,T) = P_{mc}^i(E)P_c^{i-1}(E,T). \qquad (5)$$

142 See Ref. (Higo et al., 2012) for details.

143

144 **V-McMD**

145 V-McMD introduces a virtual system, which interacts with the molecular system, and the
146 multicanonical ensemble is calculated for the entire system consisting of these two subsystems.
147 (Higo, Umezawa & Nakamura, 2013) In practice, this method can be roughly interpreted as a
148 combination of McMD and the simulated tempering method. The simulated tempering method
149 replaces the system temperature with the Metropolis criterion and performs a canonical
150 simulation until the next replacement trial. On the other hand, in V-McMD, the potential energy
151 space is split into several regions (Figure S1), and the molecular system is trapped in one of these
152 regions. With a certain time interval (t_{VST}), the molecular system replaces the region to be
153 trapped. The state variable governing which region traps the molecular system is called the
154 "virtual state," and the system defined by the virtual state is called the "virtual system." The
155 energy range of each virtual state is defined to be overlapped with the adjacent virtual states.

156   When the molecular system has the potential energy E_k in the overlapped region of the ith and
157    $(i+1)^{th}$ virtual states, the state transition between these two virtual states can occur. Because this
158   transition does not change the atomic coordinates or potential energy, the Metropolis criterion of
159   this state transition is always satisfied. The time interval of virtual-state transitions (t_{VST}) should
160   be determined arbitrarily by users. See Ref. (Higo, Umezawa & Nakamura, 2013) for details.
161
162   **TTP**
163   According to the theory of TTP, trajectories of multiple independent McMD runs with the same
164   molecular system and different initial conditions can be treated as a single trajectory of an
165   McMD simulation by concatenating the trajectories in an arbitrary order. This theory requires the
166   condition that the initial coordinates of each run are sampled from the multicanonical
167   distribution. Because the initial coordinates of production runs can be obtained from the near-
168   uniform potential energy distribution generated by iterative simulations, it is expected that this
169   condition holds. The McMD method with the TTP theory, which is called the TTP-McMD
170   method, can be considered as a hybrid Monte Carlo sampler, by assuming that the system
171   transitions from the last snapshot of the ith run (the microscopic state m_{il}) to the first snapshot of
172   the jth run (the microscopic state m_{jf}) via a Monte Carlo step (Figure S2). See Ref. (Ikebe et al.,
173   2010) for details.
174
175   **Simulation protocol**
176   We studied the three molecular systems, which are Trp-cage, PGA8, and PGA20 in an explicitly
177   solvated cubic periodic boundary cell, by using the TTP-V-McMD method. Random coil
178   structures of Trp-cage, PGA8, and PGA20 were constructed using the Modeller software (Webb
179   & Sali, 2016) without any template. The termini of the PGAs were capped with acetyl and N-
180   methyl groups, and the termini of the Trp-cage were not capped. Each of these molecular models
181   was plased into a cubic box filled by water molecules; the number of water molecules were
182   5,097, 2,879, and 3,800 for Trp-cage, PGA8, and PGA20, respectively. In addition, a Cl$^-$ ion was
183   added to the Trp-cage model to cancel the net charge of the system. The net charge of the PGA
184   models was zero because all the Glu residues were protonated.
185   The system was relaxed by using the GROMACS software. (Pronk et al., 2013) Energy
186   minimizations were successively applied using the steepest descent and conjugate gradient
187   methods. Then, an MD simulation under a constant-pressure ensemble with the Berendsen
188   barostat was performed for 1 ns. In the first half of the simulation, gradual heating from 10 to
189   300 K was applied. In the simulation, the positions of the heavy atoms of the Trp-cage were
190   restrained, the bond lengths were not constrained, and the integration time step (Δt) was 0.5 fs.
191   Subsequently, an additional constant-pressure relaxation was applied for 1 ns with $\Delta t = 2.0$ fs,
192   and the covalent bonds to hydrogen atoms were constrained using the LINCS method. (Hess et
193   al., 1997; Hess, 2008) The final configuration of each model was used for the TTP-V-McMD
194   simulations. The cell dimensions of these configurations were 54.0378 Å, 44.6116 Å, and
195   49.1174 Å for Trp-cage, PGA8, and PGA20, respectively.

196   For each model, the following steps were performed using our MD simulation program,
197   which is called myPresto/omegagene and is tailored for GE simulations. (Kasahara et al., 2016)
198   The protein conformation was randomized with a constant-temperature simulation at 800 K. By
199   using 30 snapshots taken from a trajectory with an interval of 300 ps, 30 independent runs were
200   simulated with a gradual decrease in the temperature from 629 to 296 K to estimate the density
201   of states. Successively, the TTP-V-McMD simulations were iteratively performed while
202   updating the estimation of the density of states. (Higo, Umezawa & Nakamura, 2013) A total of
203   84 production runs were performed (N_{run} = 84) for each of three different interval times for the
204   virtual-state transitions (t_{VST}) meaning the interval times for bias-potential replacement: t_{VST} =
205   0.002 ps, t_{VST} = 0.2 ps, and t_{VST} = 20 ps. The simulation length of each run (t_{run}) was 50 ns except
206   for the Trp-cage model with t_{VST} = 0.2 ps, t_{run}, of which the simulation length was 200 ns. In
207   total, 50.4 µs of trajectories were simulated as production runs. The virtual system was divided
208   into seven states that cover the energy range corresponding to the canonical distribution from
209   296 to 629 K (Table S1). The velocity scaling method (Berendsen et al., 1984) was applied to
210   maintain the system temperature.
211   For the potential parameters, the AMBER ff99SB-ILDN force field, (Lindorff-Larsen et
212   al., 2010) the ion parameter presented by Joung and Cheatham, (Joung & Cheatham, 2008) and
213   the TIP3P water model (Jorgensen et al., 1983) were applied. The electrostatic potential was
214   calculated using the zero-multipole summation method, which is a non-Ewald scheme. (Fukuda,
215   2013; Fukuda, Kamiya & Nakamura, 2014) The zero-dipole condition with the damping factor α
216   = 0 was used. (Fukuda, Yonezawa & Nakamura, 2011; Fukuda et al., 2012)
217

218   **Comparison of simulated ensembles among different settings**
219   On the basis of the trajectories obtained from of the TTP-V-McMD production runs, the effects
220   of the simulation conditions, i.e., the time interval for bias-strength replacement (t_{VST}), the
221   number of independent runs (N_{run}), and the simulation time of each run (t_{run}), were assessed.
222   For the Trp-cage model, we analyzed the FEL for various conformational ensembles on the basis
223   of the two structural parameters: the root-mean-square deviation (RMSD) of Cα atoms from the
224   native conformation (PDB ID: 1L2Y, model 1), which is denoted as $RMSD_{native}$, and the radius of
225   gyration (R_g). The FEL is visualized as the map of the potential of mean forces (PMF) on the
226   plane defined by these two parameters. We defined the *reference* ensemble as the ensemble
227   calculated for the conditions of t_{run} = 200 ns, N_{run} = 84, and t_{VST} = 0.2 ps, because it is expected
228   to have the highest reliability owing to its abundance of samples (it comprises a total of 16.8 µs
229   of simulations). The FELs analyzed in various conditions were compared with the reference FEL
230   with regard to the Pearson correlation coefficient of the PMF (PCC_{PMF}). To calculate the
231   PCC_{PMF} for a pair of FELs, bins without samples in one of the two FELs were ignored. In
232   addition, the probability of the existence of the native conformations in each ensemble (P_{native})
233   was measured to characterize each ensemble. The native conformations are defined as the
234   conformations with $RMSD_{native} \leq 2.0$ Å.

235   For the PGA models, the FELs were analyzed using principal component analysis (PCA)
236   based on the Cα–Cα distances (28 and 190 dimensions for PGA8 and PGA20, respectively). The
237   PCAs were performed using aggregations of trajectories with all the three t_{VST} conditions for
238   each model. For each t_{VST} condition, the ensemble calculated from the entire trajectory ($t_{run} = 50$
239   ns and $N_{run} = 84$) was considered as the reference ensemble. The FELs were compared with
240   regard to PCC_{PMF}, similar to the Trp-cage case.
241   To assess the effects of N_{run} and t_{run}, PCC_{PMF} (and P_{native} for the Trp-cage model) were
242   calculated for ensembles with subsets of the reference trajectories. Because there are many
243   possibilities to pick N_{run} runs from 84 runs and t_{run}-length trajectories from the entire set of
244   trajectories, we analyzed them by using the bootstrap approach. We constructed an ensemble by
245   taking a random sampling of N_{run} runs from 84 runs with replacement and repeated it 100 times.
246   The statistics over the 100 ensembles were analyzed via simulation with this N_{run} setting. This
247   process was repeatedly performed for $N_{run} = 1, 2, ..., 84$. For the case of t_{run}, the trajectories were
248   split into 5-ns bins, and an ensemble was constructed by taking a random sampling of $t_{run}/5$ bins
249   with replacement. We confirmed that the results of the bootstrap analyses with 100 and 200
250   samples were consistent (Figure S3).
251   The sampling efficiency was measured in terms of the frequency of traversals between
252   low- and high-energy regions, which were defined as the ranges $[E_{min}, E_{low}]$ and $[E_{high}, E_{max}]$,
253   respectively. Here, E_{min} and E_{max} denote the minimum and maximum potential energies in all the
254   trajectories, respectively, and E_{low} and E_{high} are defined as follows.

$$E_{low} = E_{min} + X(E_{max} - E_{min}) \tag{6}$$

$$E_{high} = E_{max} - X(E_{max} - E_{min}) \tag{7}$$

257   X is an arbitrary parameter in the range of 0 to 0.5. We assessed $X = 0.2$ and 0.3. The traversal
258   frequency $F_{travers}^{E}$ was calculated as the number of traversals between the two energy regions
259   during 1.0 ns. The traversal frequencies of $RMSD_{native}$ and R_g ($F_{travers}^{RMSD}$ and $F_{travers}^{Rg}$,
260   respectively) were also analyzed.

261

262 Results

263   In the first part of this section, the results of the Trp-cage model are described. The reference
264   ensemble is characterized in the subsection, "FEL of folding–unfolding equilibrium of Trp-
265   cage". Next, the effects of the parameters t_{run}, N_{run}, and their balances are discussed in the
266   successive subsections: "Effects of simulation time for each run," "Effects of number of
267   independent runs," and "Balance between simulation time and number of runs," respectively.
268   Subsequently, the effects of the other parameter t_{VST} are discussed in the subsection, "Effects of
269   frequency of bias-strength replacement." Additionally, the following subsection, "Effects of
270   system complexity" describes the results of the PGA8 and PGA20 models and compares them
271   with those of the Trp-cage model.

272

273 FEL of folding–unfolding equilibrium of Trp-cage

274   For the Trp-cage model, we performed 34 iterations of TTP-V-McMD simulations while
275   updating the estimation of the density of states, $n(E)$, and obtained a near-uniform energy
276   distribution (Figure S4). On the basis of this estimation, we performed production runs with N_{run}
277   $= 84$, $t_{run} = 200$ ns, and $t_{VST} = 0.2$ ps. This is called the reference setting hereinafter. The resultant
278   canonical ensemble reweighted at 300 K is referred to as the reference ensemble.
279   The FEL of the reference ensemble projected on the $RMSD_{native}$–R_g plane is shown in
280   Figure 1A. The most stable basin corresponds to the native structure consisting of an α-helix at
281   the N-terminus, a 3_{10}-helix at the middle, and a loop region at the C-terminus (the secondary
282   structural elements were recognized by using the DSSP software) (Kabsch & Sander, 1983). For
283   example, the $RMSD_{native}$ of one of the most probable structures in this basin was 0.994 Å (Figure
284   1B). The energy barrier (approximately 3.3 kcal/mol) was observed at $RMSD_{native} \approx 3$ Å in a low-
285   R_g regime. Around this barrier, the 3_{10}-helix at the middle of the peptide chain was partially
286   deformed; this deformation can be the first step of an unfolding process (Figure 1C). The details
287   of the unfolding pathway are not discussed in this paper. The second basin was widely spread
288   around $RMSD_{native} = 4$–7 Å and $R_g = 7$–9 Å. This corresponds to the unfolded state, and examples
289   of the unfolded structures taken from this basin are shown in Figures 1E and F. The difference in
290   the PMF between the bottoms of the first and second stable basins was 1.014 kcal/mol, and the
291   population of the native conformations (P_{native}) was 22.37%. The landscape is qualitatively
292   similar to that calculated using the REMD method reported by another group (Day, Paschek &
293   Garcia, 2010). Our TTP-V-McMD simulation successfully identified the native structure as the
294   most stable basin in the energy landscape, by using the reference setting.
295
296   **Effects of simulation time for each run**
297   The FELs of the Trp-cage model were drawn for a variety of t_{run} values under the condition of
298   $N_{run} = 84$ and compared with the reference FEL. The FELs based on the trajectories of 0–25, 0–
299   50, and 0–100 ns are shown in Figures 2A, B, and C, respectively. The overall geometries of
300   these FELs were qualitatively similar to the reference (Figure 1A); their PCC_{PMF} values were
301   0.936, 0.936, and 0.994, respectively. The bootstrap statistics of PCC_{PMF} for each t_{run} value are
302   summarized in Figure 2D. For $t_{run} = 200$ ns, the bootstrap average and the standard deviation
303   (SD) of PCC_{PMF} were 0.990 and 0.007, respectively. Even in the worst case among 100
304   randomly generated ensembles with $t_{run} = 200$ ns, PCC_{PMF} was 0.966. From this condition, a
305   decrease in t_{run} yielded a slow decay of PCC_{PMF}, and PCC_{PMF} reached 0.9 at $t_{run} \approx 30$ ns, which
306   corresponds to 15% of the samples in the reference. Further decreasing t_{run} resulted in a steep
307   decrease of PCC_{PMF}. Along with the decrease of the bootstrap average of PCC_{PMF}, the SD was
308   increased. This means that an insufficient simulation time causes a loss of robustness of the
309   results.
310   In contrast to the fact that the PCC_{PMF} decays in a shorter t_{run} than the reference, the
311   balance between the folded and unfolded states (P_{native}) was almost constant regardless of t_{run}
312   (Figure 2E); the bootstrap average of P_{native} for $t_{run} = 5$–200 ns was in the range of 0.220 to 0.225.
313   However, the SD of P_{native} was reduced with the increase of t_{run}; the SDs of P_{native} at $t_{run} = 5$, 50,

314 and 200 ns were 0.07, 0.02, and 0.008, respectively. The loss of robustness due to the
315 insufficiency of the simulation time is demonstrated in terms of not only the similarity of the
316 entire FEL but also the stability of the native fold.
317
318 **Effects of number of independent runs**
319 As in the previous subsection, the effects of the reduction of N_{run} on the FELs were assessed
320 under the condition of $t_{run} = 200$ ns. Examples of FELs with $N_{run} = 10$, 21, and 42 are shown in
321 Figures 3A, B, and C, respectively; the PCC_{PMF} values were 0.637, 0.939, and 0.993,
322 respectively. Although the positions and wideness of the basins were similar to the reference, the
323 FELs with a smaller N_{run} were smoother and lacked small bumps on the landscapes. The
324 bootstrap statistics of PCC_{PMF} for various N_{run} values (Figure 3D) were similar to those for t_{run}
325 (Figure 2D). The quantity of the samples required for $PCC_{PMF} \geq 0.9$ was approximately one-
326 fourth of the reference ($N_{run} \approx 21$). The average (and the SD) of PCC_{PMF} at $N_{run} = 21$ and 42 were
327 0.906 (0.07) and 0.956 (0.04), respectively. Larger N_{run} values are needed to obtain robust
328 results.
329   Regarding P_{native}, the influence of the reduction of N_{run} (Figure 3E) differed from that of
330 the reduction of t_{run} (Figure 2E). A lower N_{run} resulted in the underestimation of the population of
331 native conformations. P_{native} reached at plateau for $N_{run} \geq 21$. A certain number of runs was
332 needed to obtain robust results, and $t_{run} = 200$ ns was too short to reach equilibrium with a small
333 number of trajectories for this system.
334
335 **Balance between simulation time and number of runs**
336 The evaluation for various t_{run} values with $N_{run} = 84$ runs (Figure 2) and that for various N_{run}
337 values with $t_{run} = 200$ ns (Figure 3) indicate that reducing t_{run} produced better results than
338 reducing N_{run} if the cumulative simulation time ($N_{run} \times t_{run}$) was the same. Figure 4 shows direct
339 comparisons of the results, indicating that high-N_{run} conditions resulted in a higher PCC_{PMF} and
340 more similar values of P_{native} to the reference, with lower SDs, than long-t_{run} conditions. In
341 particular, the qualitative difference between the two strategies is shown by the mean of P_{native}.
342 Reducing N_{run} resulted in the significant underestimation of the fold stability, but reducing t_{run}
343 did not.
344   In addition, we performed bootstrap analyses for all the combinations of 40-t_{run} settings
345 (5, 10, 15, ..., 200 ns) and 21-N_{run} settings (4, 8, 12, ..., 84). The average values of PCC_{PMF} and
346 P_{native} in all the conditions are presented in Figures 5 and S5. The PCC_{PMF} was proportional to
347 $\log(N_{run} \times t_{run})$. While the trend of P_{native} is ambiguous, the use of a larger number of samples
348 resulted in a higher P_{native}. In the case where only small amount of data was available, a lower
349 ratio of t_{run}/N_{run} (purple plots in Figure 5) yielded better results.
350
351 **Effects of frequency of bias-strength replacement**
352 The parameter t_{VST} controls the frequency of the bias-strength switching in the TTP-V-McMD
353 method. We investigated the effects of this parameter by comparing the TTP-V-McMD

354 simulations of the Trp-cage model under the three conditions—t_{VST} = 0.002, 0.2, and 20 ps—
355 with t_{run} = 50 ns for N_{run} = 84.
356   Table 1 summarizes the frequency of traversals between high- and low-potential energy
357 regimes ($F_{trv}{}^E$), as defined in Eqs. (6) and (7) with X = 0.3 and 0.2, as well as the frequency of
358 traversals between $RMSD_{native}$ ($F_{trv}{}^{RMSD}$) and R_g ($F_{trv}{}^{Rg}$). The simulations with a shorter t_{VST}
359 resulted in faster traversals in the potential energy space, indicating that with a shorter t_{VST}, a
360 wider potential energy range can be sampled in a shorter time. However, faster traversal in the
361 potential energy space does not ensure faster transition of the protein conformation. For both X =
362 0.2 and 0.3, although the setting of t_{VST} = 0.002 ps yielded the highest $F_{trv}{}^E$, this condition did not
363 yield a higher $F_{trv}{}^{RMSD}$ and $F_{trv}{}^{Rg}$ compared to when a longer t_{VST} was used. This result indicates
364 that the relaxation of the conformation requires a longer time than that of the potential energy. If
365 a strong bias is applied and the system takes a high-potential energy state, it can return to low-
366 energy states before conformational changes. Therefore, a moderate speed for traversals in the
367 potential energy space is ideal for efficient conformational sampling. In the case of X = 0.2, t_{VST}
368 = 0.2 ps exhibited the most frequent conformational changes.
369   In addition, the resultant ensembles were slightly affected by the setting of t_{VST}. We
370 analyzed P_{native} for ensembles of various t_{run} values with N_{run} = 84 using the bootstrap method
371 (Figure S6). The results for all three t_{VST} values showed similar trends, i.e., near-constant average
372 values and the gradual decay of the SD with the increase of t_{run}. While t_{VST} = 0.2 ps showed a
373 smaller P_{native} than the other two t_{VST} settings, the difference was smaller than the SD. On the
374 other hand, higher SD values were observed in the following order: t_{VST} = 0.2 > 20 > 0.002 ps.
375 This is consistent with the order of $F_{trv}{}^{RMSD}$ and $F_{trv}{}^{Rg}$ (Table 1). The result indicates that more
376 frequent traversals between high- and low-$RMSD_{native}$ conformations make it possible to explore
377 a wider region of the conformational space; thus, the population of the native conformation
378 decreases, and the SD increases.
379   Regarding the PCC_{PMF} with the reference setting (t_{VST} = 0.2 ps, N_{run} = 84, and t_{run} = 200
380 ns), the average PCC_{PMF} values at t_{run} = 50 ns differed among different settings of t_{VST} (Figure
381 S6). This indicates that changing t_{VST} yields subtle differences in the resultant ensemble.
382 Regarding the balance between t_{run} and N_{run}, the trends were similar for all the settings of t_{VST}
383 (Figure S7).
384
385 **Effects of system complexity: comparison with the PGA models**
386 We performed the same analyses for the molecular models of PGA8 and PGA20. In contrast to
387 Trp-cage, these peptides did not exhibit a particular fold. The FELs of both PGA8 and PGA20
388 were unimodal distributions, the basins of which consisted of a variety of collapsed
389 conformations (Figure 6 for t_{VST} = 0.2 ps). The ensembles included short secondary structural
390 elements but they were unstable. Although the shape of the small bumps in the basins differed
391 depending on the simulation conditions, the overall geometries of the FELs were similar (Figure
392 S8 for t_{VST} = 0.002 ps and 20 ps).

393   Regarding the balance between t_{run} and N_{run}, Figure 7 shows the bootstrap averages of
394   PCC_{PMF} between the ensemble calculated by the full-length trajectory (t_{run} = 50 ns and N_{run} = 84)
395   and those calculated by the reduced trajectories. No clear differences were found between the
396   PCC_{PMF} curve with reduced t_{run} and that with reduced N_{run} for both the PGA8 and PGA20
397   (Figure 7 for t_{VST} = 0.2 ps; Figure S9 for the other conditions). A small number of long
398   simulations exhibited the similar efficiency as that of many short simulations. In addition, no
399   significant differences were found between the results of PGA8 and PGA20. It is noteworthy that
400   the conformational space of PGA20 is considerably wider than that of PGA8 and similar to that
401   of Trp-cage, because the conformational space volume of polypeptides is determined primarily
402   by their length, Therefore, we concluded that the effects of balance between t_{run} and N_{run} are
403   determined by the complexity of the FEL (e.g., existence of the free-energy barrier) rather than
404   the conformational space volume. An increase in the number of runs is more effective for a
405   system with more complex FEL.
406   For the PGA models, the frequencies of traversals in the potential energy and R_g spaces
407   ($F_{trv}{}^{E}$ and $F_{trv}{}^{Rg}$, respectively) are summarized in Table 2. Both the PGA8 and PGA20 models
408   yielded similar trends as the Trp-cage model (Table 1). Although frequent replacements of bias-
409   potential strength enhanced the traversals in the potential energy space, they did not enhance the
410   conformational changes in terms of R_g. This implies that the conformational changes are much
411   slower than the potential energy changes even if there is no free-energy barrier exists in the
412   landscape. However, in contrast to the Trp-cage case, the drawback of the frequent replacement,
413   that is, slow traversals in the conformational space, is unclear in the case of PGA20.
414

Discussion

416   We examined the performance of the TTP-V-McMD method with regard to two adjustable
417   settings: (i) the balance between the number of runs (N_{run}) and the simulation length in each run
418   (t_{run}) and (ii) the frequency of the bias-strength switching (t_{VST}). For (i), in the Trp-cage model
419   including folding–unfolding transition, we found higher robustness of the conditions with a
420   larger number of runs than with longer simulations. In particular, the probability of the existence
421   of native conformations in a resultant ensemble (P_{native}) was more sensitive to the condition than
422   the entire similarity of the FEL. However, for the cases of PGAs without free-energy barrier in
423   their FELs, no significant effect was shown in the balance between the number and length of
424   simulations. Therefore, the optimal balance depended on the molecular system, and the
425   complexity of the FELs was a key feature rather than the degree of freedom. In any case,
426   increasing the number of simulations was recommended because it is not worse than increasing
427   the length of each run. This result is practically useful because performing many parallel runs is
428   easier than executing a single long simulation. While the result obtained here encourages
429   performing many short runs, it requires the condition that the initial structures of the production
430   runs are uniformly sampled from the multicanonical ensemble, whose energy distribution is
431   uniform. (Ikebe et al., 2010) As our protocol samples the initial structures of the production runs
432   from the previous iteration of the McMD, it is expected that this condition holds.

433   For (ii), whereas higher frequencies of bias-strength replacement enhance the sampling of
434   a wider range of potential energy, they do not ensure the enhancement of the sampling of a wider
435   range of conformations. This means that the enhancement of the sampling along one variable
436   (e.g., potential energy or temperature) does not ensure the enhancement of the sampling along
437   another variable (e.g., RMSD and R_g). Rapid traversals in the energy space sometimes obtain a
438   high energy and return to the low-energy regime before conformational change regardless of the
439   existence of free-energy barrier in the FEL. A moderate frequency is needed to maximize the
440   performance for any molecular system.

441   The findings that we obtained by applying the TTP-V-McMD method provide insight
442   into the characteristics of many other GE methods. (i) For GE methods that involve running
443   independent parallel simulations, e.g., simulated tempering and AUS, performing many short
444   runs can be more effective than increasing the length of each run. For GE methods where parallel
445   runs are coupled, e.g., the REMD method, this conclusion should not be simply applied. For
446   example, an increase in the number of runs in the REMD method resulted in larger overlaps of
447   the distributions of neighboring replicas, along with an increase in the acceptance probability of
448   replica-exchange trials. Our previous evaluation for the REMD method showed that a larger
449   number of replicas does not always yield better results. (Iwai, Kasahara & Takahashi, 2018) The
450   number of runs should be adjusted independently from the coupling condition of the parallel
451   runs; for example, the number of runs in a REMD simulation could be increased by performing
452   two or more independent REMD simulations with different initial conformations, and
453   aggregating the resultant ensembles. (ii) Regarding the frequency of the bias-strength
454   replacement, the conclusion that the interval should be long enough to relax the conformation
455   could be transferred to other GE methods. For the REMD methods, the effects of the interval for
456   replica-exchange trials have been reported; while some studies recommended shorter intervals
457   (Sindhikara, Meng & Roitberg, 2008; Sindhikara, Emerson & Roitberg, 2010), the side effects of
458   highly frequent exchange trials have also been reported and were consistent to our result (Periole
459   & Mark, 2007; Iwai, Kasahara & Takahashi, 2018).

460

461

462

Conclusions

464   In this study, the effects of two parameters of GE methods, i.e., (i) the balance between the
465   number of runs (N_{run}) and the simulation length in each run (t_{run}) and (ii) the frequency of the
466   bias-strength switching (t_{VST}) were extensively examined with using all-atom explicit-solvent
467   models of three polypeptides that are a foldable mini-protein and disordered peptides. We
468   suggest a guide to adjust the setting for general molecular systems and GE methods. (i)
469   Increasing in the number of runs should be prioritized rather than increasing the simulation
470   length. (ii) Highly frequent replacements of the bias potentials may yield side effects because
471   conformational relaxation was slower than potential energy relaxation. The time interval for
472   replacement should be longer than or equal to 0.2 ps.

473

Acknowledgements

474 The MD simulations were performed using the TSUBAME3 supercomputer at the Tokyo
475 Institute of Technology, provided through the HPCI System Research Projects (Project IDs:
476 hp180050, hp180054, hp190017, and hp190018). The numerical computations for post-
477 simulation analyses were performed using the supercomputer system provided by the National
478 Institute of Genetics, Research Organization of Information and Systems, Japan.
479

480

References

482 Abraham MJ, Murtola T, Schulz R, Páll S, Smith JC, Hess B, Lindahl E 2015. GROMACS:
483   High performance molecular simulations through multi-level parallelism from laptops to
484   supercomputers. *SoftwareX* 1-2:19–25.
485 Ahmed Z, Beta IA, Mikhonin AV, Asher SA 2005. UV−Resonance Raman Thermal Unfolding
486   Study of Trp-Cage Shows That It Is Not a Simple Two-State Miniprotein. *Journal of the*
487   *American Chemical Society* 127:10943–10950. DOI: 10.1021/ja050664e.
488 Berendsen HJC, Postma JPM, van Gunsteren WF, DiNola A, Haak JR 1984. Molecular
489   dynamics with coupling to an external bath. *Journal of Chemical Physics* 81:3684–3690.
490   DOI: 10.1063/1.448118.
491 Clarke DT, Doig AJ, Stapley BJ, Jones GR 1999. The alpha-helix folds on the millisecond time
492   scale. *Proceedings of the National Academy of Sciences of the United States of America*
493   96:7232–7237. DOI: 10.1073/pnas.96.13.7232.
494 Day R, Paschek D, Garcia AE 2010. Microsecond simulations of the folding/unfolding
495   thermodynamics of the Trp-cage miniprotein. *Proteins: Structure, Function, and*
496   *Bioinformatics* 78:1889–1899. DOI: 10.1002/prot.22702.
497 Donten ML, Hamm P 2013. pH-jump induced α-helix folding of poly-l-glutamic acid. *Chemical*
498   *Physics* 422:124–130. DOI: 10.1016/j.chemphys.2012.11.023.
499 Finke JM, Jennings PA, Lee JC, Onuchic JN, Winkler JR 2007. Equilibrium unfolding of the
500   poly(glutamic acid)20 helix. *Biopolymers* 86:193–211. DOI: 10.1002/bip.20719.
501 Fukuda I 2013. Zero-multipole summation method for efficiently estimating electrostatic
502   interactions in molecular system. *The Journal of chemical physics* 139:174107. DOI:
503   10.1063/1.4827055.
504 Fukuda I, Kamiya N, Nakamura H 2014. The zero-multipole summation method for estimating
505   electrostatic interactions in molecular dynamics: Analysis of the accuracy and application to
506   liquid systems. *The Journal of chemical physics* 140:194307. DOI: 10.1063/1.4875693.
507 Fukuda I, Kamiya N, Yonezawa Y, Nakamura H 2012. Simple and accurate scheme to compute
508   electrostatic interaction: Zero-dipole summation technique for molecular system and
509   application to bulk water. *The Journal of Chemical Physics* 137:054314. DOI:
510   10.1063/1.4739789.
511 Fukuda I, Yonezawa Y, Nakamura H 2011. Molecular dynamics scheme for precise estimation
512   of electrostatic interaction via zero-dipole summation principle. *The Journal of Chemical*
513   *Physics* 134:164107. DOI: 10.1063/1.3582791.
514 Hałabis A, Żmudzińska W, Liwo A, Ołdziej S 2012. Conformational Dynamics of the Trp-Cage
515   Miniprotein at Its Folding Temperature. *The Journal of Physical Chemistry B* 116:6898–
516   6907. DOI: 10.1021/jp212630y.
517 Hess B 2008. P-LINCS: A Parallel Linear Constraint Solver for Molecular Simulation. *Journal*

518   *of Chemical Theory and Computation* 4:116–122. DOI: 10.1021/ct700200b.

519 Hess B, Bekker H, Berendsen HJC, Fraaije JGEM 1997. LINCS: a linear constraint solver for
520   molecular simulations. *Journal of computational chemistry* 18:1463–1472.

521 Higo J, Dasgupta B, Mashimo T, Kasahara K, Fukunishi Y, Nakamura H 2015. Virtual-system-
522   coupled adaptive umbrella sampling to compute free-energy landscape for flexible molecular
523   docking. *Journal of computational chemistry* 36:1489–1501. DOI: 10.1002/jcc.23948.

524 Higo J, Ikebe J, Kamiya N, Nakamura H 2012. Enhanced and effective conformational sampling
525   of protein molecular systems for their free energy landscapes. *Biophysical Reviews* 4:27–44.
526   DOI: 10.1007/s12551-011-0063-6.

527 Higo J, Umezawa K, Nakamura H 2013. A virtual-system coupled multicanonical molecular
528   dynamics simulation: Principles and applications to free-energy landscape of protein–protein
529   interaction with an all-atom model in explicit solvent. *The Journal of Chemical Physics*
530   138:184106. DOI: 10.1063/1.4803468.

531 Ikebe J, Umezawa K, Kamiya N, Sugihara T, Yonezawa Y, Takano Y, Nakamura H, Higo J
532   2010. Theory for trivial trajectory parallelization of multicanonical molecular dynamics and
533   application to a polypeptide in water. *Journal of computational chemistry* 32:1286–1297.
534   DOI: 10.1002/jcc.21710.

535 Iwai R, Kasahara K, Takahashi T 2018. Influence of various parameters in the replica-exchange
536   molecular dynamics method: Number of replicas, replica-exchange frequency, and
537   thermostat coupling time constant. *Biophysics and Physicobiology* 15:165–172. DOI:
538   10.2142/biophysico.15.0_165.

539 Jani V, Sonavane UB, Joshi R 2014. REMD and umbrella sampling simulations to probe the
540   energy barrier of the folding pathways of engrailed homeodomain. *Journal of Molecular*
541   *Modeling* 20:2283. DOI: 10.1007/s00894-014-2283-8.

542 Jorgensen WL, Chandrasekhar J, Madura JD, Impey RW, Klein ML 1983. Comparison of simple
543   potential functions for simulating liquid water. *The Journal of chemical physics* 79:926–935.
544   DOI: 10.1063/1.445869.

545 Joung IS, Cheatham TE 2008. Determination of Alkali and Halide Monovalent Ion Parameters
546   for Use in Explicitly Solvated Biomolecular Simulations. *The Journal of Physical Chemistry*
547   *B* 112:9020–9041. DOI: 10.1021/jp8001614.

548 Kabsch W, Sander C 1983. Dictionary of protein secondary structure: Pattern recognition of
549   hydrogen-bonded and geometrical features. *Biopolymers* 22:2577–2637. DOI:
550   10.1002/bip.360221211.

551 Kasahara K, Ma B, Goto K, Dasgupta B, Higo J, Fukuda I, Mashimo T, Akiyama Y, Nakamura
552   H 2016. myPresto/omegagene: a GPU-accelerated molecular dynamics simulator tailored for
553   enhanced conformational sampling methods with a non-Ewald electrostatic scheme.
554   *Biophysics and Physicobiology* 13:209–216. DOI: 10.2142/biophysico.13.0_209.

555 Kimura T, Takahashi S, Akiyama S, Uzawa T, Ishimori K, Morishima I 2002. Direct
556   Observation of the Multistep Helix Formation of Poly- l-glutamic Acids. *Journal of the*
557   *American Chemical Society* 124:11596–11597. DOI: 10.1021/ja026639f.

558 Lindorff-Larsen K, Piana S, Palmo K, Maragakis P, Klepeis JL, Dror RO, Shaw DE 2010.
559   Improved side-chain torsion potentials for the Amber ff99SB protein force field. *Proteins:*
560   *Structure, Function, and Bioinformatics* 78:1950–1958. DOI: 10.1002/prot.22711.

561 Nakajima N, Nakamura H, Kidera A 1997. Multicanonical Ensemble Generated by Molecular
562   Dynamics Simulation for Enhanced Conformational Sampling of Peptides. *The Journal of*
563   *Physical Chemistry B* 101:817–824. DOI: 10.1021/jp962142e.

564 Ogasawara N, Kasahara K, Iwai R, Takahashi T 2018. Unfolding of α-helical 20-residue poly-
565   glutamic acid analyzed by multiple runs of canonical molecular dynamics simulations. *PeerJ*
566   6:e4769. DOI: 10.7717/peerj.4769.
567 Periole X, Mark AE 2007. Convergence and sampling efficiency in replica exchange simulations
568   of peptide folding in explicit solvent. *Journal of Chemical Physics* 126:014903. DOI:
569   10.1063/1.2404954.
570 Péter Hudáky, Pál Stráner, Viktor Farkas, Györgyi Váradi, Gábor Tóth A, András Perczel 2007.
571   Cooperation between a Salt Bridge and the Hydrophobic Core Triggers Fold Stabilization in
572   a Trp-Cage Miniprotein†. *Biochemistry* 47:1007–1016. DOI: 10.1021/bi701371x.
573 Pronk S, Páll S, Schulz R, Larsson P, Bjelkmar P, Apostolov R, Shirts MR, Smith JC, Kasson
574   PM, van der Spoel D, Hess B, Lindahl E 2013. GROMACS 4.5: a high-throughput and
575   highly parallel open source molecular simulation toolkit. *Bioinformatics (Oxford, England)*
576   29:845–854. DOI: 10.1093/bioinformatics/btt055.
577 Rosta E, Hummer G 2009. Error and efficiency of replica exchange molecular dynamics
578   simulations. *Journal of Chemical Physics* 131:165102. DOI: 10.1063/1.3249608.
579 Salomon-Ferrer R, Götz AW, Poole D, Le Grand S, Walker RC 2013. Routine Microsecond
580   Molecular Dynamics Simulations with AMBER on GPUs. 2. Explicit Solvent Particle Mesh
581   Ewald. *Journal of Chemical Theory and Computation* 9:3878–3888. DOI:
582   10.1021/ct400314y.
583 Shaw DE, Grossman JP, Bank JA, Batson B, Butts JA, Chao JC, Deneroff MM, Dror RO, Even
584   A, Fenton CH, Forte A, Gagliardo J, Gill G, Greskamp B, Ho CR, Ierardi DJ, Iserovich L,
585   Kuskin JS, Larson RH, Layman T, Lee L-S, Lerer AK, Li C, Killebrew D, Mackenzie KM,
586   Mok SY-H, Moraes MA, Mueller R, Nociolo LJ, Peticolas JL, Quan T, Ramot D, Salmon
587   JK, Scarpazza DP, Ben Schafer U, Siddique N, Snyder CW, Spengler J, Tang PTP, Theobald
588   M, Toma H, Towles B, Vitale B, Wang SC, Young C 2014. Anton 2: raising the bar for
589   performance and programmability in a special-purpose molecular dynamics supercomputer.
590   In: IEEE Press, 41–53. DOI: 10.4324/9780203843550.
591 Shirts MR, Chodera JD 2008. Statistically optimal analysis of samples from multiple equilibrium
592   states. *The Journal of chemical physics* 129:124105. DOI: 10.1063/1.2978177.
593 Sindhikara DJ, Emerson DJ, Roitberg AE 2010. Exchange Often and Properly in Replica
594   Exchange Molecular Dynamics. *Journal of chemical theory and computation* 6:2804–2808.
595   DOI: 10.1021/ct100281c.
596 Sindhikara D, Meng Y, Roitberg AE 2008. Exchange frequency in replica exchange molecular
597   dynamics. *The Journal of chemical physics* 128:024103. DOI: 10.1063/1.2816560.
598 Souaille M, Roux B 2001. Extension to the weighted histogram analysis method: combining
599   umbrella sampling with free energy calculations. *Computer Physics Communications*
600   135:40–57.
601 Sugita Y, Okamoto Y 1999. Replica-exchange molecular dynamics method for protein folding.
602   *Chemical Physics Letters* 314:141–151.
603 Webb B, Sali A 2016. Comparative Protein Structure Modeling Using MODELLER. *Current
604   protocols in bioinformatics / editoral board, Andreas D. Baxevanis ... [et al.]* 54:5.6.1–
605   5.6.37. DOI: 10.1002/cpbi.3.
606

Figure 1

FEL calculated by the reference ensemble of Trp-cage.

(A) FEL based on the $RMSD_{native}$–R_g plane. The color gradation indicates the PMF. (B) Snapshot taken from the first basin (blue) superimposed on the experimentally solved structure (gray; PDB ID: 1Y2L, model 1). (C) Examples of snapshots near the first basin. The structures colored dark cyan and light cyan correspond to the positions C1 and C2 marked in (A), respectively. (D, E) Examples of unfolded structures in the second basin. The positions of each snapshot on the FEL are marked in (A).
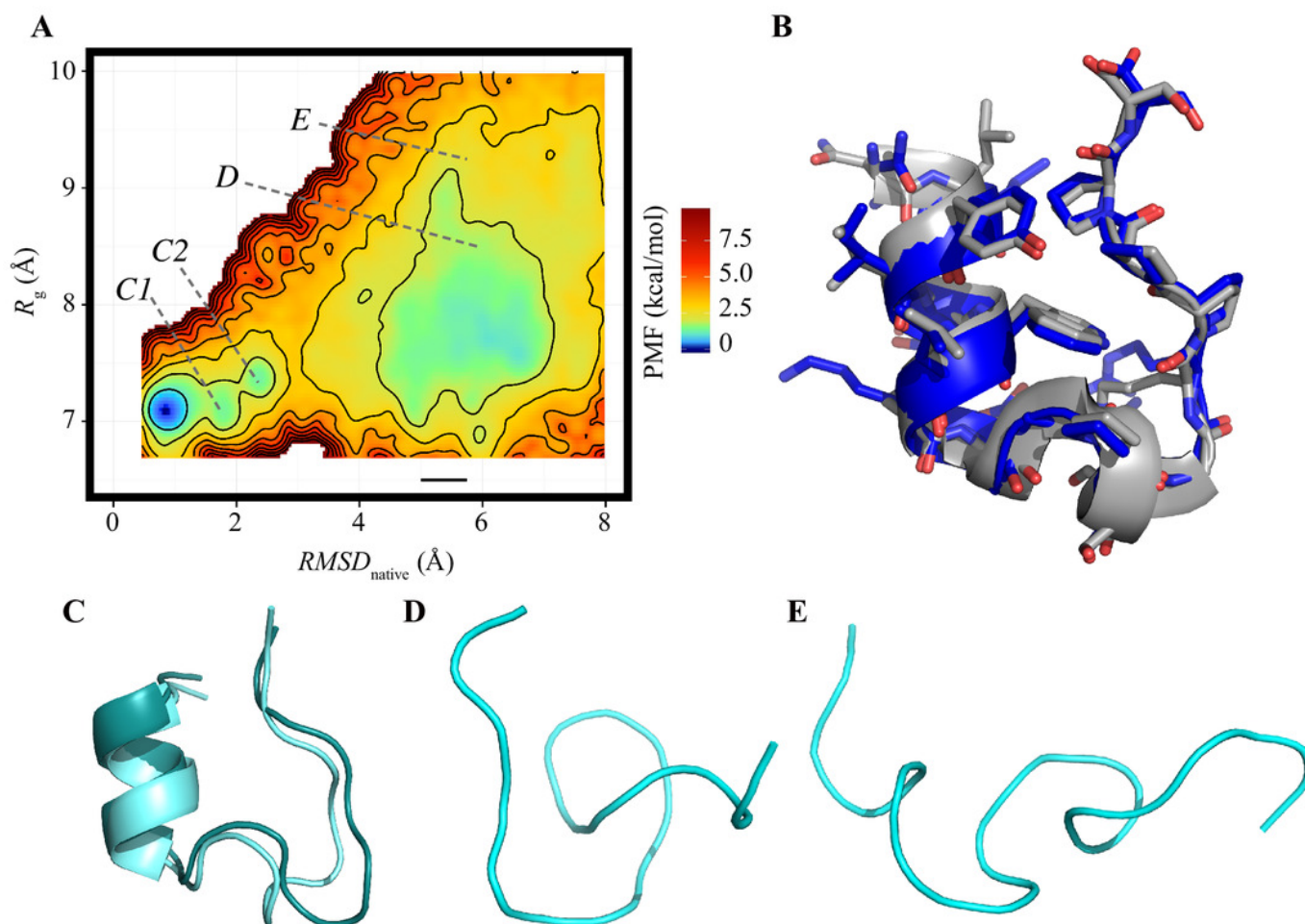
Figure 2

FELs of Trp-cage for various t_{run} values with N_{run} = 84.

(A, B, C) FELs based on the trajectories of 0–25 ns (A), 0–50 ns (B), and 0–100 ns (C). (D) Bootstrap statistics of PCC_{PMF}. The solid line is the average, the dashed lines are the sum of the average and SD and the subtraction of the SD from average. The dotted lines indicate the maximum and minimum values among 100 randomly generated ensembles in each condition. (E) Statistics of P_{native} shown in the same scheme as (D).
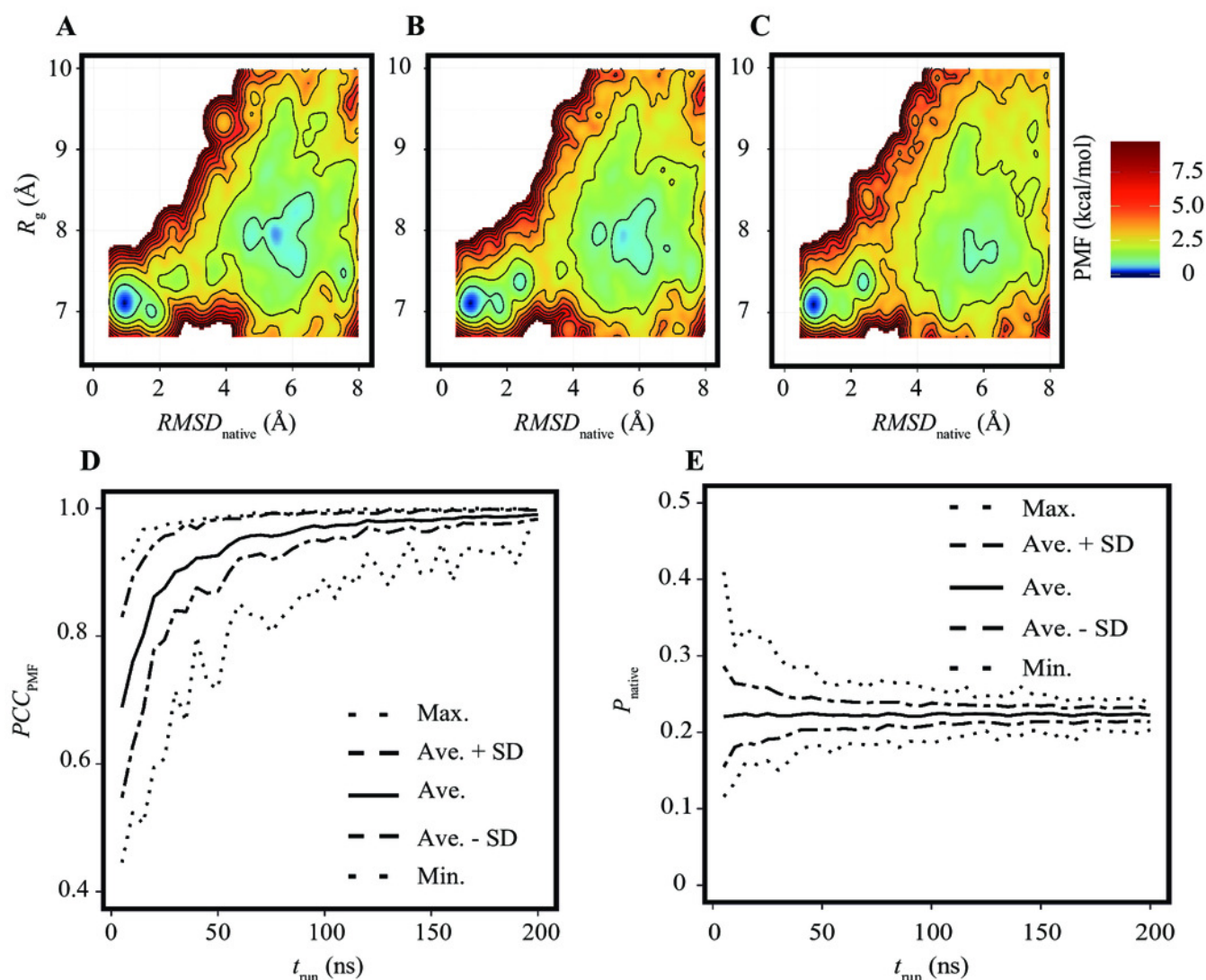
Figure 3

Characteristics of FELs of Trp-cage for smaller N_{run} values with t_{run} = 200 ns.

(A, B, C) Examples of FELs with N_{run} = 10 (A), N_{run} = 21 (B), and N_{run} = 42 (C). (D, E) Bootstrap statistics of PCC_{PMF} (D) and P_{native} (E). See also the legend of Figure 2.
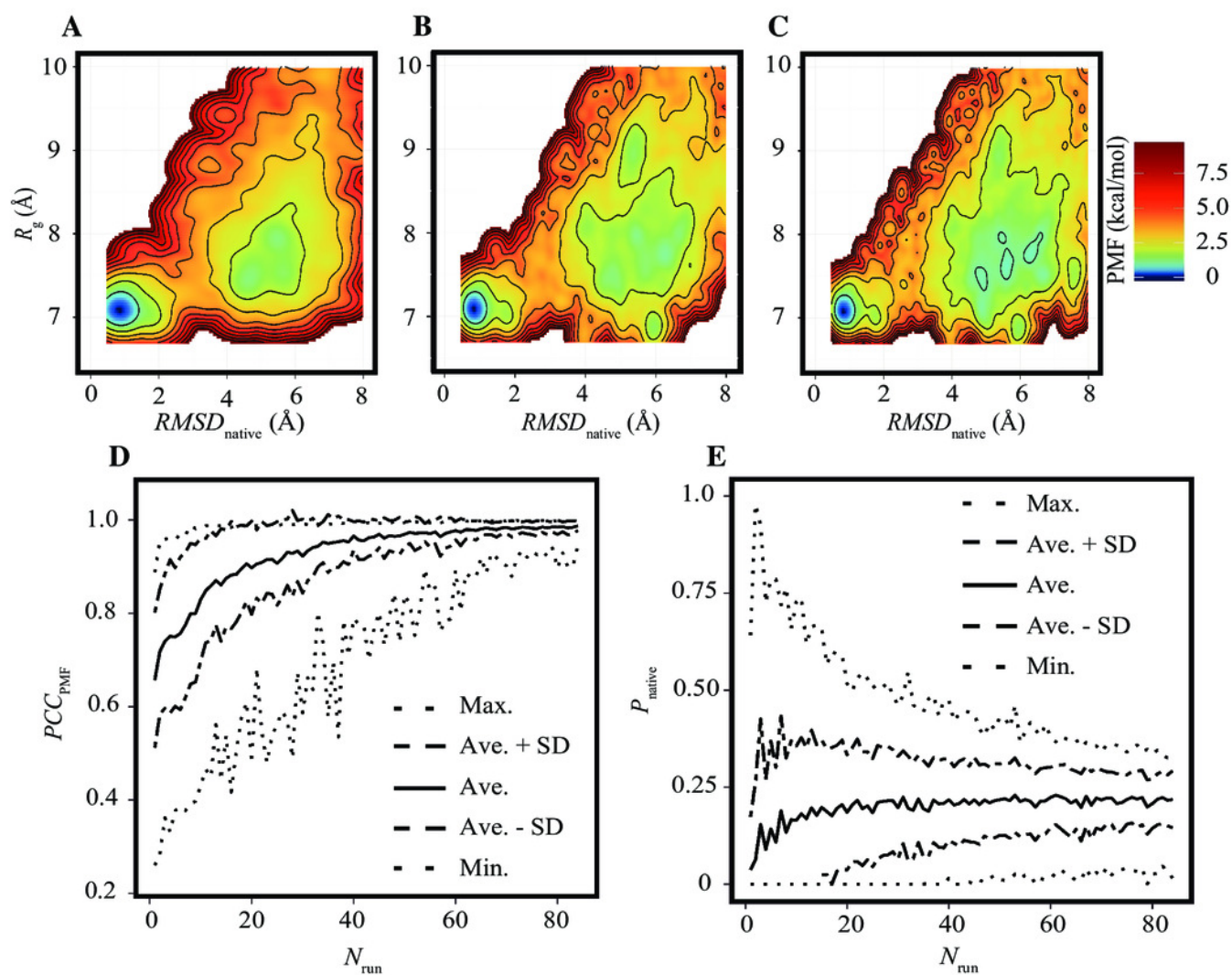
Figure 4

Direct comparison between reducing t_{run} with the fixed-N_{run} condition (blue line) and reducing N_{run} with the fixed-t_{run} condition (red line) for the Trp-cage model.

The vertical axes indicate (A) the average of PCC_{PMF}, (B) the SD of PCC_{PMF}, (C) the average of P_{native}, and (D) the SD of P_{native}. The horizontal axis indicates the accumulated simulation length ($N_{run} \times t_{run}$).
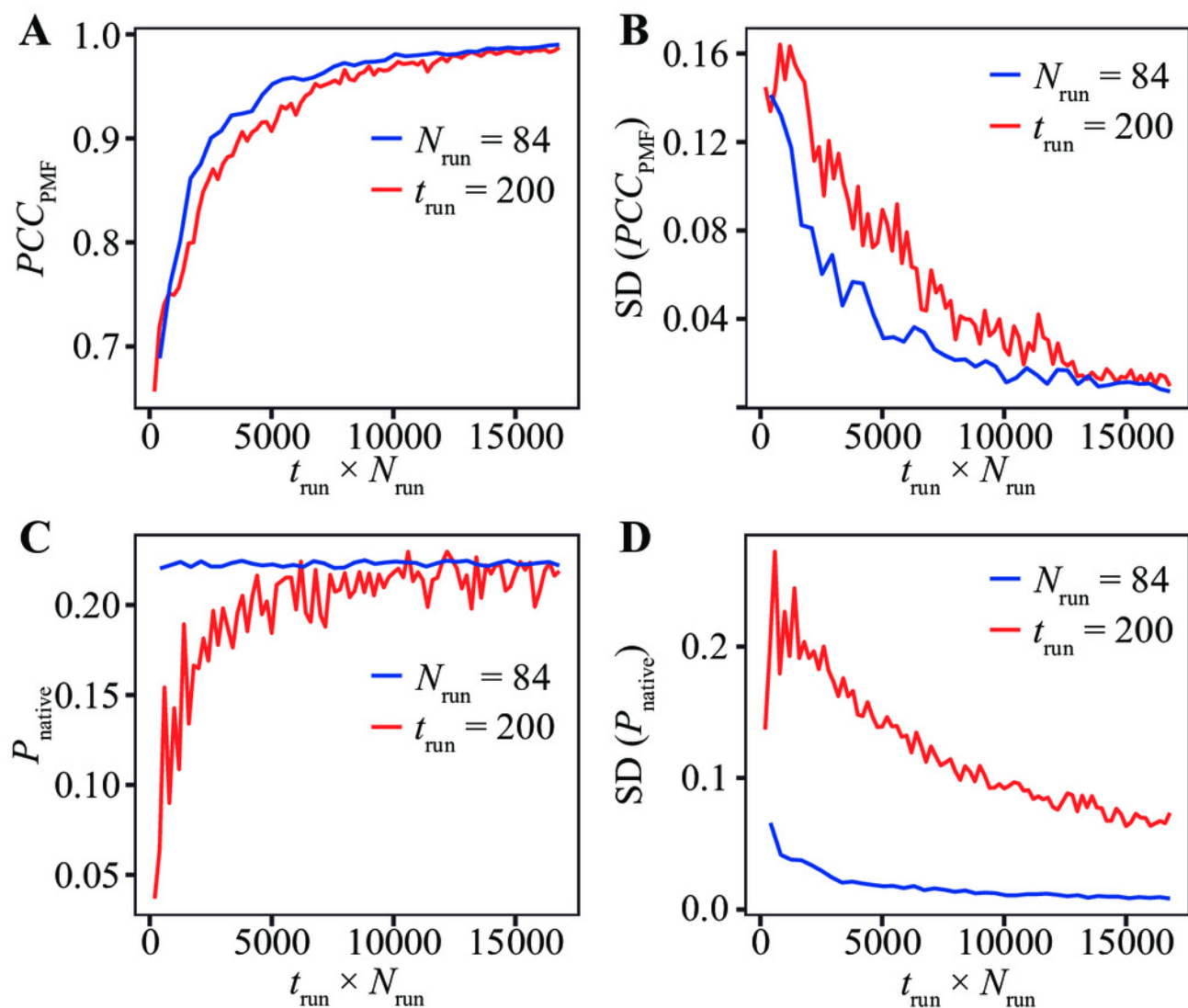
Figure 5

Distribution of (A) the average of PCC_{PMF} and (B) P_{native} along the logarithm of the accumulated simulation length for various combinations of N_{run} and t_{run} extracted from the trajectories th

The color of each plot indicates the log-ratio of N_{run} to t_{run} compared with the reference. The definition is $\log[(t_{run}/N_{run})/(200/84)]$. This value becomes greater than 0 for conditions with a higher ratio of t_{run} to N_{run} than the reference.
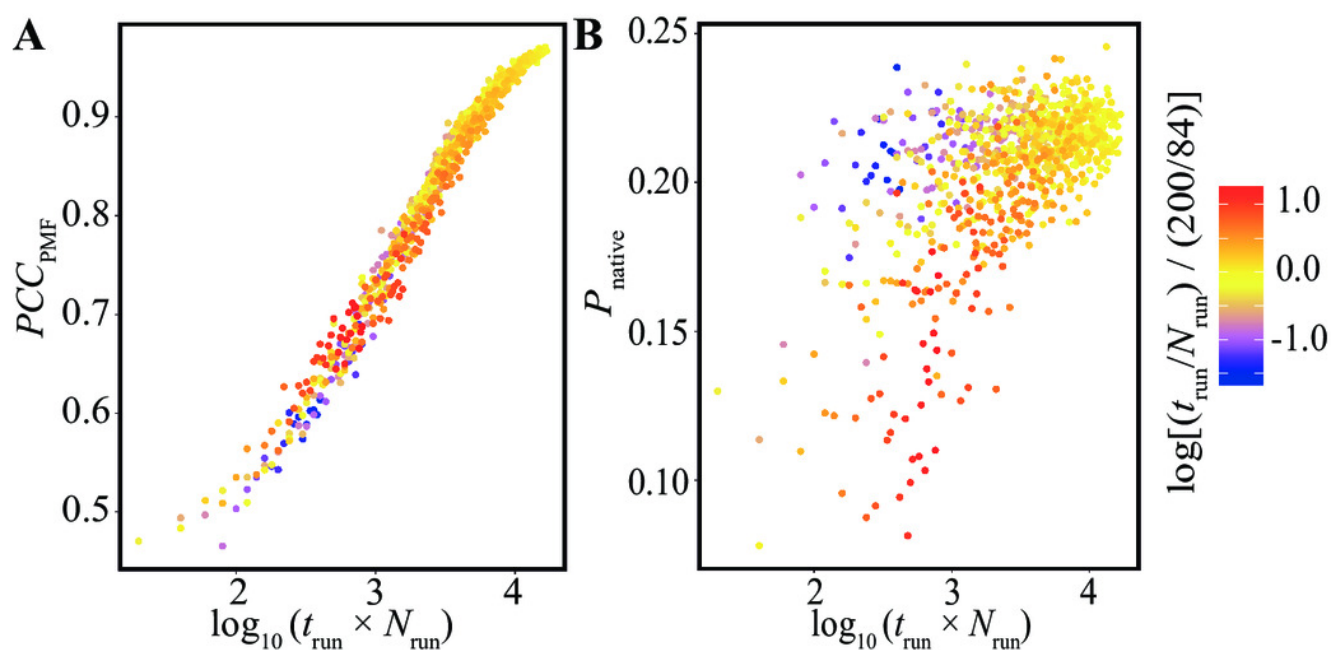
Figure 6

FELs calculated by ensembles of (A) PGA8 and (B) PGA20 using t_{run} = 50 ns and N_{run} = 84 with t_{VST} = 0.2 ps.

(C, D, E) Examples of snapshots in the basins marked in the panels (A) and (B).
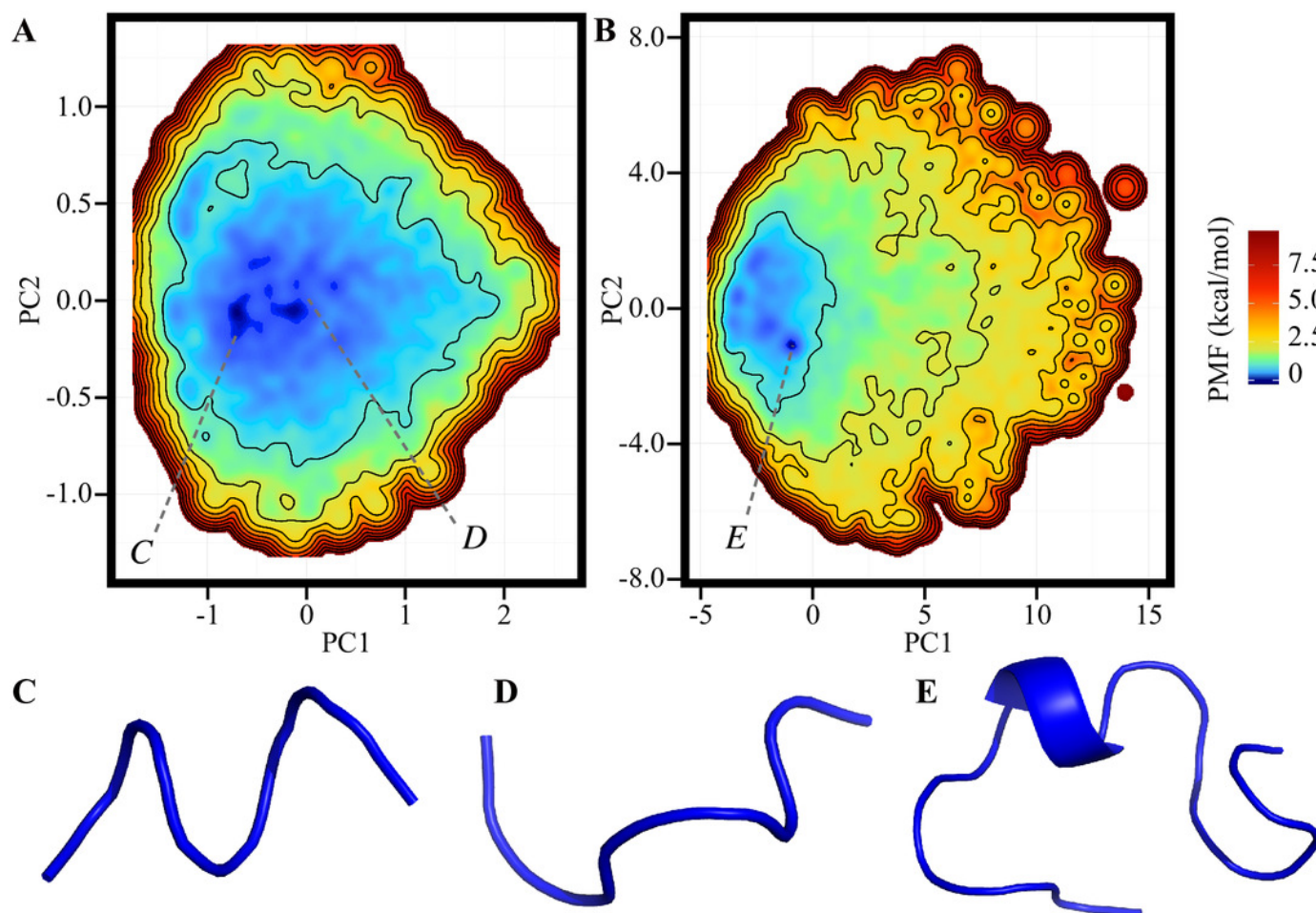
Figure 7

Direct comparisons between reducing t_{run} with fixed-N_{run} (blue line) and reducing N_{run} with fixed-t_{run} (red line) for (A, B) the PGA8 and (C, D) PGA20 systems.

The vertical axes indicate (A, C) the bootstrap average of PCC_{PMF}, and (B, D) the SD of PCC_{PMF}. The horizontal axis indicates the accumulated simulation length ($N_{run} \times t_{run}$). The results of t_{VST} = 0.2 ps are presented. See also Figure S9 for the other t_{VST} conditions.
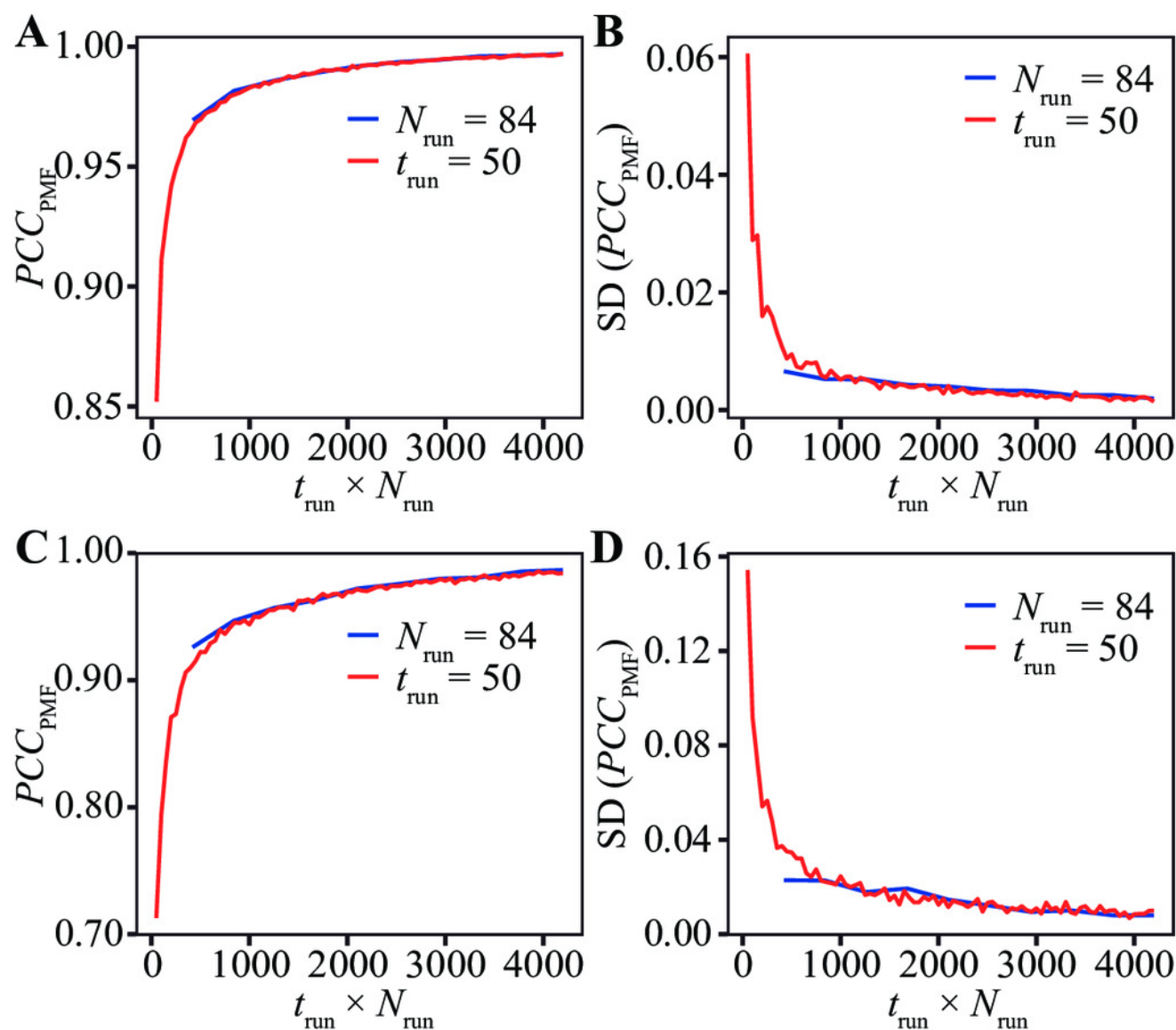
Average values (and the standard errors) of the traversal frequencies over 84 runs for the Trp-cage model.

1   **Table 1.** Average values (and the standard errors) of the traversal frequencies over 84 runs for the

2   Trp-cage model.

t_{VST} (ps)	0.002	0.2	20
X		0.3	
$F_{trv}{}^{E}$ (ns^{-1})	1.63 (0.06)	1.45 (0.04)	1.02 (0.04)
$F_{trv}{}^{RMSD}$ (ns^{-1})	0.057 (0.006)	0.060 (0.004)	0.062 (0.006)
$F_{trv}{}^{Rg}$ (ns^{-1})	0.040 (0.005)	0.044 (0.003)	0.050 (0.006)
X		0.2	
$F_{trv}{}^{E}$ (ns^{-1})	0.70 (0.03)	0.62 (0.02)	0.46 (0.02)
$F_{trv}{}^{RMSD}$ (ns^{-1})	0.005 (0.001)	0.011 (0.001)	0.006 (0.002)
$F_{trv}{}^{Rg}$ (ns^{-1})	0.008 (0.002)	0.012 (0.001)	0.007 (0.002)

Average values (and standard errors) of the traversal frequencies over 84 runs for PGA models.

1   **Table 2.** Average values (and standard errors) of the traversal frequencies over 84 runs for PGA

2   models.

Model	PGA8			PGA20		
t_{VST} (ps)	0.002	0.2	20	0.002	0.2	20
X	0.3			0.3		
F_{trv}^{E} (ns^{-1})	2.91	2.70	0.86	1.05	0.99	0.46
	(0.03)	(0.03)	(0.02)	(0.04)	(0.03)	(0.02)
F_{trv}^{Rg} (ns^{-1})	0.44	0.47	0.47	0.045	0.044	0.049
	(0.02)	(0.02)	(0.02)	(0.005)	(0.005)	(0.006)
X	0.2			0.2		
F_{trv}^{E} (ns^{-1})	1.58	1.53	0.50	0.4	0.41	0.22
	(0.02)	(0.02)	(0.01)	(0.02)	(0.01)	(0.01)
F_{trv}^{Rg} (ns^{-1})	0.117	0.147	0.146	0.011	0.013	0.015
	(0.007)	(0.007)	(0.007)	(0.002)	(0.002)	(0.003)